



Ytterbium tungstate nanoparticles as a novel sorbent for basic dyes from aqueous solutions

Ali Zeraatkar Moghaddam¹  · Majid Kalate Bojdi¹ · Alireza Nakhaei¹ ·
Mohammad Reza Ganjali^{2,3} · Taher Alizadeh⁴ · Farnoush Faridbod²

Received: 12 January 2018 / Accepted: 12 July 2018 / Published online: 17 July 2018
© Springer Nature B.V. 2018

Abstract

Ytterbium tungstate nanoparticles (YTNP) were used as a sorbent for removing methylene blue (MB), as a model cationic dye, from water solutions. YTNPs were characterized through scanning electron microscopy. The factors influencing the efficiency of the sorbent in a batch adsorption procedure (i.e., initial pH, amount of YTNPs, and contact time) were evaluated at a constant concentration of MB, and central composite design was used to determine their efficacies. The results indicated the best conditions in the case of a 200-ppm MB solutions to be 3 mg mL⁻¹ (as the amount of YTNPs used), pH = 10, and contact time = 30 min. The adsorption kinetics, isotherm and desorption properties of YTNPs were also fully investigated. The Langmuir model was used for fitting the adsorption isotherm and the results indicated a high adsorption capacity for the model dye. The adsorption kinetics was found to comply with a pseudo-second-order behavior, which means that adsorption constitutes the rate-determining step. Furthermore, YTNPs were successfully used to remove MB from water and wastewater samples.

Keywords Removal · Cationic dye · Ytterbium tungstate nanoparticles · Experimental design · Isotherm · Kinetics

✉ Ali Zeraatkar Moghaddam
a_zeraatkar_m@birjand.ac.ir

¹ Department of Chemistry, Faculty of Sciences, University of Birjand, Birjand, Iran

² Center of Excellence in Electrochemistry, University of Tehran, Tehran, Iran

³ Endocrinology and Metabolism Research Center, Tehran University of Medical Sciences, Tehran, Iran

⁴ Department of Analytical Chemistry, Faculty of Chemistry, University College of Science, University of Tehran, Tehran, Iran

Introduction

Organic dyes are used in various areas ranging from the textile, leather, pulp and paper industries to the plastic, cosmetic, printing, food processing, and pharmaceutical industries. Consequently, the compounds are widely discharged into the environment through industrial wastewaters [1, 2]. Consequently, there is a huge demand for developing tools and methods for eliminating these pollutants before their discharge. The common synthetic dyes (especially azo dyes) are not biodegradable, due to the presence of aromatic sections in their structures, and hence survive they approaches like aerobic digestion and oxidation. On the other hand, the majority of these dyes are toxic or carcinogenic and cause severe harm to aquatic organisms [3]. It is noteworthy that every year about 1 million tons of azo dyes are produced and over 2000 different types of the dyes are currently in use [4]. The various methods conventionally used for treating dye-containing effluents are coagulation/flocculation [5], photodegradation [6], ion exchange [7], membrane filtration [8], electrochemical treatment [9], biological treatment [10] and adsorption [11]. These methods are usually cost-intensive and/or complicated [12].

However, adsorption techniques constitute low-cost and environmentally friendly tools and have hence been reported as appropriate and convenient [13–15] which have therefore led to the development of a wide range of sorbents [16], while studies on preparing low-cost high-capacity sorbents are still on-going [17, 18]. Examples include the application of activated carbon [19, 20], as well as various different nanomaterials as highly potential compounds for use as sorbents, due to their unique properties [21, 22].

Nanotechnology offers various promises and the application of nano-scale particles has become an attractive area in recent years. An example can be the use of nano-sized adsorbents in wastewater treatment applications. Up to now, many different nano-based adsorbents have been explored to remove dyes from wastewater.

Lanthanide-based salts have recently been synthesized as nanoparticles [23–33]. Tungstate and molybdate salts of lanthanides constitute important families of materials with various applications in phosphors, optical fibers, scintillators, magnets and catalysts [31, 34, 35]. Furthermore, rare earth tungstates have been associated with different advantages [36]. Pr^{3+} ion salts, for instance, offer distinct properties [35], and its tungstate [37], vanadate [38], molybdenate [39], and titanate [40] have been prepared and used. Given the importance of the surface area of synthesized particles, and because the specific surface area of the materials naturally increases with reducing their particle sizes, the number of active sites present at the surface of such materials can be enhanced, which can lead to improved absorption capacities.

Various tungstate-based nanoparticles have recently been reported [28–32, 35, 41–46], and the focus of this work is on the application of synthesized ytterbium tungstate nanoparticles (YTNP) for removing methylene blue (MB), as a model cationic synthetic dye, from water samples. The YTNPs were synthesized through a direct precipitation reaction [35] and their composition and

morphological properties were found to be satisfactory without the need for the application of surface active compounds, templates or catalysts. Reviewing the related literature revealed no reports on the application of YTNP for the adsorptive removal of MB. The parameters influencing the removal process were optimized through central composite design (CCD) and response surface methodology, and the adsorption isotherm and kinetics were also evaluated under optimum conditions, and the optimal procedure eventually used for removing MB from water and wastewater samples.

Experimental

Chemicals and instruments

MB (99.8%), ytterbium (III) chloride anhydrous and sodium tungstate dihydrate were obtained from Sigma–Aldrich (St. Louis, MO, USA), and the analytical grade solvents were supplied by Merck (Darmstadt, Germany).

An ultrasonic bath (Eurosonic 4D ultrasonic cleaner) with a frequency of 50 kHz and an output power of 350 W was used to disperse materials in the aqueous samples. A UV–Vis spectrophotometer (Specord 210 Plus; Analytik Jena, Germany) was employed to determine the concentration of MB.

Synthesis of YTNPs

Ultra-fine particles of ytterbium(III) tungstate were synthesized by the addition of an aqueous solution of Yb^{3+} (0.005 M) with feeding flow rates of 40 mL min^{-1} to the tungstate aqueous solution (0.005 M) under vigorous stirring at reactor temperatures of $30 \text{ }^\circ\text{C}$. After complete mixing of the reagents in the reactor, the precipitated YTNPs were filtered and washed with distilled water three times in order to remove the remained soluble ions on the surface of the precipitated particles. Thereafter, the obtained precipitate was washed with absolute ethanol and dried at $80 \text{ }^\circ\text{C}$ for 4 h (Fig. 1).

The chemical composition of the prepared product was studied by X-ray powder diffraction (XRD) and the results (Fig. 2) showed that the XRD pattern of the nanoparticles is in good agreement with that of ytterbium tungsten oxide obtained from the PC-APD diffraction software (No. 00-023-1482).

A Fourier-transform infrared (FTIR) analysis of the product was also performed to characterize its chemical structure and moisture content (Fig. 3). The results contained several wide absorption peaks at about 716, 793, 827, 918, 967, 1632 and 3415 cm^{-1} , the last two of which were attributed, respectively, to the stretching and bending of the O–H and H–O–H bonds of the surface-absorbed H_2O [47].

Also, a scanning electron microscopy (SEM) image of the synthesized YTNPs is shown in Fig. 4.

Fig. 1 Fluxogram detailing the steps of the YTNPs' preparation

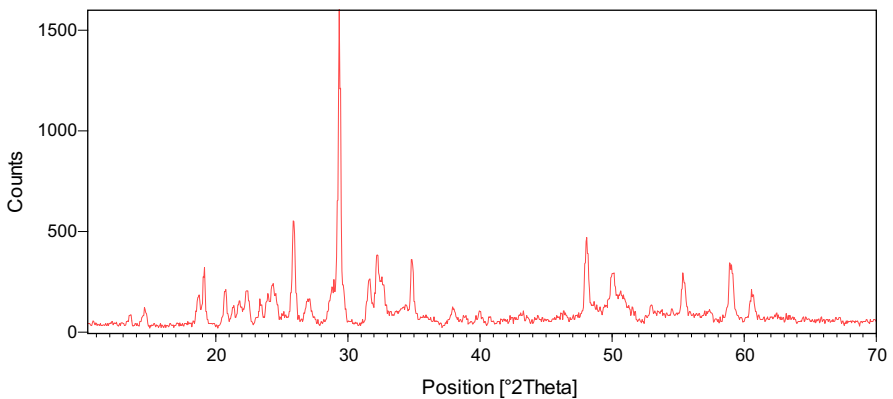
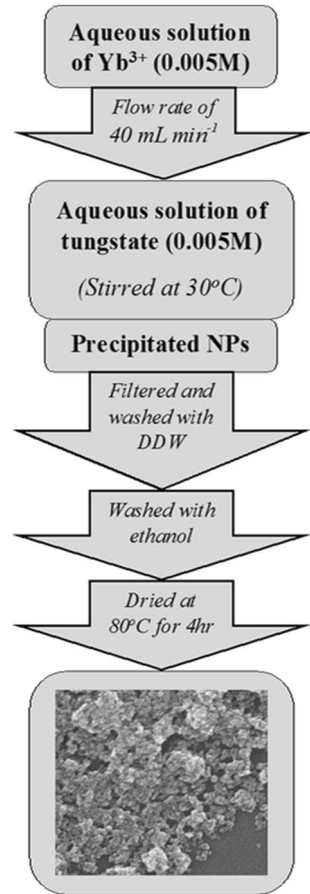


Fig. 2 XRD pattern for as-synthesized YTNPs

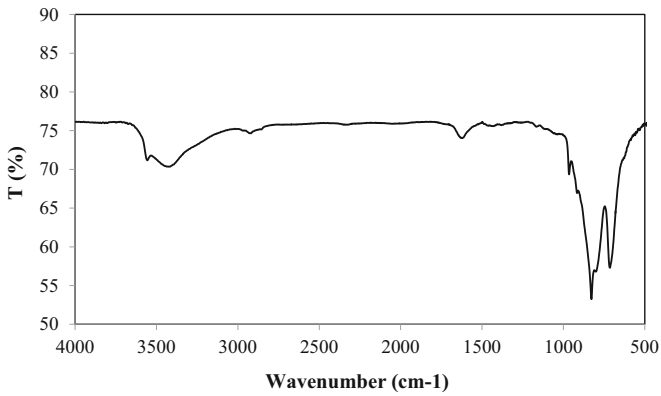


Fig. 3 FTIR spectra for YTNPs synthesized in optimum conditions

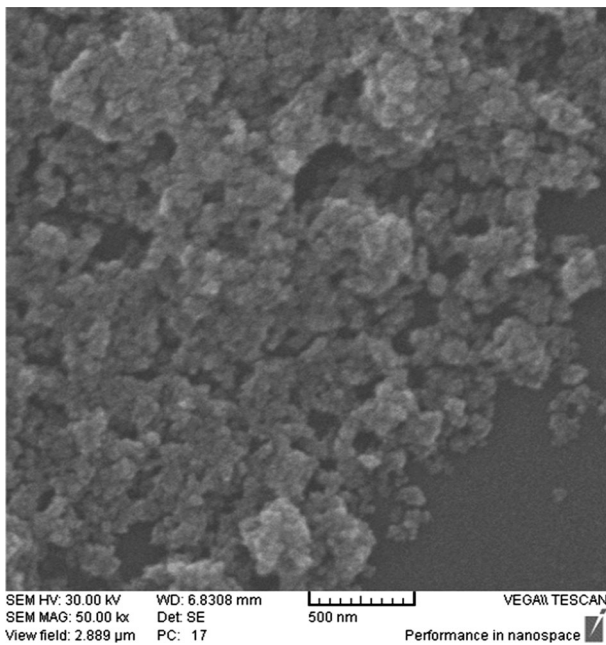


Fig. 4 SEM image of the synthesized YTNPs

Batch adsorption studies

As mentioned before, the YTNPs were used in a batch mode to remove MB, and the effects of different parameters, i.e., the amount of the YTNPs in the range of 0.32–3.7 mg mL⁻¹; the initial pH of the solution in the range of 6–11; and the contact time in the range of 20–70 min, were monitored using a 200-ppm solution of MB at 25 °C while the mixture was being stirred at 700 rpm. The typical

adsorption experiment involved adding a quantity of the YTNPs to a tube containing 10 mL of the 200-ppm MB solution and adjusting the solution pH to the desired value by adding 0.01 M HCl or NaOH. The adsorption mixture was next stirred at 700 rpm for half an hour. After that, the procedure aliquots of the suspensions were taken and used for determining the MB concentration.

The isotherms were studied through performing experiments using different initial MB concentrations in the range of 50–300 ppm, under optimal conditions, and the kinetic studies were run using 200-ppm MB solutions under optimal conditions while changing the contact time (0–50 min).

The removal efficiencies and adsorption capacities at equilibrium and any arbitrary moment t (q_e and q_t , mg g⁻¹) were calculated using the equilibrium MB concentration and its concentration at time t using the following equations:

$$\text{Removal Efficiency(\%)} = \frac{C_o - C_e}{C_o} \times 100 \quad (1)$$

$$q_e = \frac{(C_o - C_e)V}{m}, \quad q_t = \frac{(C_o - C_t)V}{m} \quad (2)$$

in which C_o , C_e and C_t represent the concentrations of MB in the sample solution in mg L⁻¹ before the adsorption, under equilibrium conditions and at time t , V (L) is the volume of the sample solution and m (g) is the mass of YTNPs. The C_o , C_e and C_t were determined using Beer's law and the UV–Vis absorbance at $\lambda_{\text{max}} = 667$ nm.

Optimization

To reach the best removal efficiency, the factors influencing the procedure, i.e., solution pH, amount of YTNPs, and contact time were optimized while the initial MB concentration, temperature and stirring rate were constant (25 °C and 500 rpm). The first evaluations involved the effect of the nature of the sorbent on the efficiency at different pH values. This was followed by evaluating the influence of the rest of parameters, i.e., pH, MB concentration, amount of YTNPs, and contact time through CCD. The trial version of the Design Expert 9.0.0 package (Stat-Ease, Minneapolis, MN, USA) was used to perform the experimental design matrix and data analyses.

Results and discussion

Experimental design

As a common method, univariate methodology was used to optimize the procedures. However, the method requires a large number of experiments which considerably increases the required time and cost, and also does not consider the interactions between the variables. Multivariate techniques, on the other hand, are fast, efficient, and capable of simultaneously optimizing more than one variable. CCD is an independent, rotatable, orthogonal and quadratic design [48] and was applied in this work.

Furthermore, although various variables influence the adsorption of dyes, the pH, amount of the YTNPs, and contact time are most important factors in this regard and hence their effects on the adsorption efficiency (as the response) contributed to build a surface, and were probed by the CCD-based model. Finally, analysis of variance (ANOVA) was used to assess the model and to analyze the data.

Given the limited number of parameters involved, they were not screened through factorial design, and hence CCD [49] was used directly. Based on CCD, for a given number of parameters (f), the number of design points (N) required is given by Eq. 1:

$$N = 2^f + 2f + N_0 \quad (3)$$

Consequently, 36 experiments were performed based on the CCD, and the experiments were randomized into 3 blocks. The proper ranges for the parameters are presented in Table 1. The ranges for dose and time are selected based on preliminary experiments, whereas the range of pH was assigned based on available textile wastewaters as we know that most of them are alkaline. The experiments were conducted according to the design matrix offered by the software. The subsequent analyses by ANOVA and CCD produced the following second-order polynomial function:

$$\begin{aligned} \text{Removal (\%)} = & +48.03 + 20.85A + 12.47B - 3.54C - 13.50AC + 6.00BC \\ & - 1.73A^2 \end{aligned} \quad (4)$$

The response values were changed to square root values for the removal efficiency (not shown) using the Box–Cox plot.

The positive values of each term in Eq. 2 indicate a positive corresponding effect on the response, while negative values indicate the subsequent decreases.

ANOVA breaks down the overall variation into components of different sources [50], and easily estimates the effects of effects. The results of ANOVA on the MB removal efficiency data (Table 2) are based on the sums of squares applied to determine the affected parameters, as well as Fisher's F ratios and P values. A model F value of 345.67 indicates its statistical importance. This further shows that there is only a 0.01% chance for the "model F value" to occur, due to noise. The negligible value of more than 0.05 for lack of fit supports the validity of the quadratic model in explaining the experimental data [51]. The terms for the interaction of AC and BC , the quadratic A^2 term, and the linear effects of all the

Table 1 The experimental variables and levels of the BBD

Parameters	Levels				
	$\alpha-$	- 1	0	+ 1	$\alpha+$
Initial pH (A)	6	7	8.5	10	11
Dose (mg mL^{-1}) (B)	0.32	1	2	3	3.7
Contact time (min) (C)	20	30	45	60	70

Table 2 Table of ANOVA for the removal efficiency of MB using the YTNP

	Sums of squares	<i>df</i>	Mean square	<i>F</i> value	<i>p</i> value
Model	9990.99	9	1110.11	237.47	< 0.0001
Block	10.54	2	5.27		
A-pH	5894.30	1	5894.30	1260.88	< 0.0001
B-dose	2131.52	1	2131.52	455.96	< 0.0001
C-contact time	169.97	1	169.97	36.36	< 0.0001
AB	2.00	1	2.00	0.43	0.5265
AC	1458.00	1	1458.00	311.89	< 0.0001
BC	288.00	1	288.00	61.61	< 0.0001
A2	46.30	1	46.30	9.90	0.0093
B2	5.33×10^{-3}	1	5.33×10^{-3}	1.14×10^{-3}	0.9737
C2	0.071	1	0.071	0.015	0.9041
Residual	51.42	11	4.67		
Lack of fit	33.42	5	6.68	2.23	0.1788
Pure error	18.00	6	3.00		
R^2	0.9949				
Adjusted R^2	0.9907				
Predicted R^2	0.9574				
RSD (%)	4.60				

parameters were found to be significant. The significance terms are presented in Fig. 5a.

As can be seen in Table 2, the high R^2 value of 0.9949 for the removal of MB based on the model indicates an agreement between the experimental and predicted results. The predicted value for R^2 (0.9574) is consistent with the adjusted value (i.e., 0.9907). Based on the normal probability of residuals (Fig. 5b), it is understood that no serious violation from the basic assumptions of the analyses exists. The good normal distribution of the results indicates the normality of the assumptions, as well as the independence of the earlier residuals. In the plot of the residual values versus the number of experiments, the residuals show a random distribution around zero, reflecting the accuracy of the model. The ‘adequate precision’ as a criterion of the signal to noise ratio at a value greater than 4 reflects the efficiency and suitability of the method [52]. Here, the value of 53.47 shows the adequacy of the signal and the applicability of the applied model for navigating the design space.

3D plots of the model are good tools for studying the nature of the interactions [53] and presenting a visual overview of the dependencies between the responses and the parameters. The plots of the response model against two experimental factors (one held fixed at its central level, while varying the other) are illustrated in Fig. 6. Figure 6a illustrates the effect of the initial pH of the solution and the amount of the YTNPs. From this figure, it is clear that the amount of the YTNPs and pH have positive effects on the adsorption efficiency; however, the efficiency

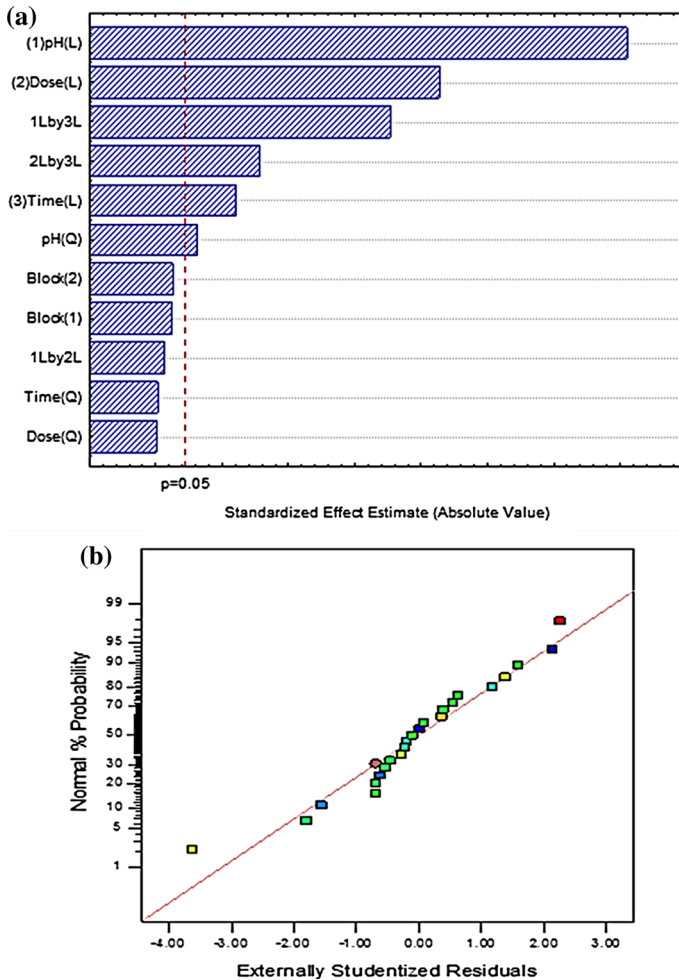


Fig. 5 **a** Pareto chart of studentized effect and **b** normal probability plot of studentized residual for MB removal efficiency

decreased over $\text{pH} = 10$. In general, raising the pH increases the electrostatic interactions between MB and YTNPs, and hence considerably increases the removal efficiency; however, at pH values over 10 the removal efficiency drops. Figure 6b clearly shows that increasing the contact time enhances the removal efficiency at low pH values, while it has the opposite effect at high pH levels, proving some sort of interdependency between the two parameters, which is further supported by the fact that the lines in this figure are not parallel. Based on Fig. 6c, there is also an interaction between the amount of YTNPs and the contact time (Fig. 6c).

Determination of the optimal values for the effective factors, with the aim of maximizing the MB removal efficiency using the obtained model as the main objective of the optimization process, was performed using a trial version of

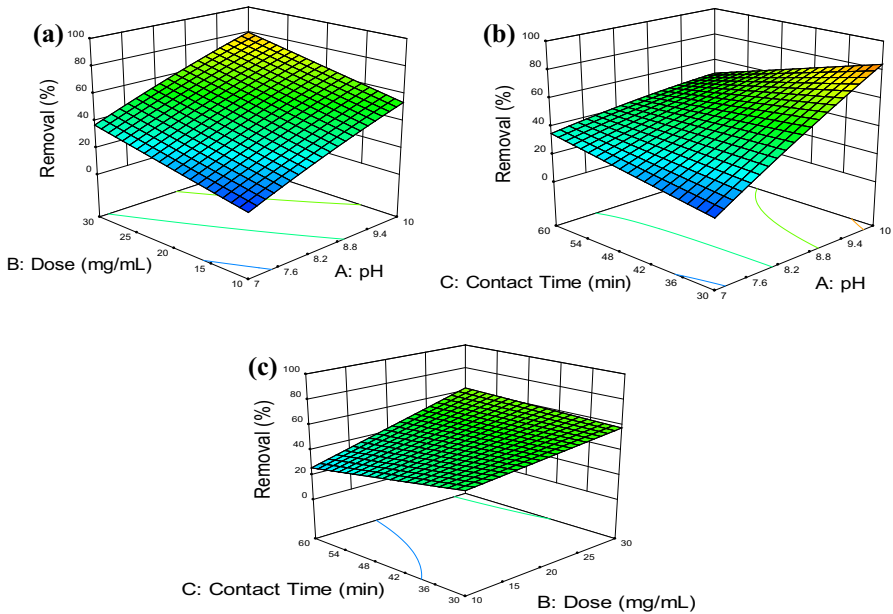


Fig. 6 The response surface plots of the effect of sample pH, amount of the YTNPs, and contact time

Design-Expert 10.0.0. Based on the Nelder–Mead non-linear optimization approach, these optimal values were determined to be 10 for pH, 3 mg mL^{-1} for the amount (dose) of the YTNPs and 30 min as the contact time, which led to a maximum predicted removal efficiency of above 90% from a 200-ppm MB solution. At a 95% confidence level, the best response was expected to be $91.2 \pm 2.2\%$, which was further verified through the results of the experiments performed under optimal conditions, which led to an experimental removal efficiency of $89.5 \pm 5.7\%$, which is very close to the predictions of the CCD model.

Kinetic studies of the adsorption

To determine the kinetic parameters, pseudo-first-order, pseudo-second-order, and Weber and Morris kinetic models were used to fit the data obtained from the experiment, and the calculated results have been summarized in Table 3. The Lagergren equation, for the capacity of solids:

Table 3 Kinetic parameters for the adsorption of MB onto YTNPs

Time range (min)	C_0 (ppm)	Pseudo-first-order			Pseudo-second-order		
		q_e (mg g^{-1})	k_1 (min^{-1})	R^2	q_e (mg g^{-1})	k_2 (min^{-1})	R^2
0–60	200	27.55	0.0744	0.6232	62.11	0.0056	0.9791

$$\ln(q_e - q_t) = \ln q_e - k_1 t \quad (5)$$

was used as the pseudo-first order model [54]. In this equation, k_1 represents the pseudo-first order rate constant, and can be calculated using the slope of the linear plot of $\ln(q_e - q_t)$ versus time (Fig. 7).

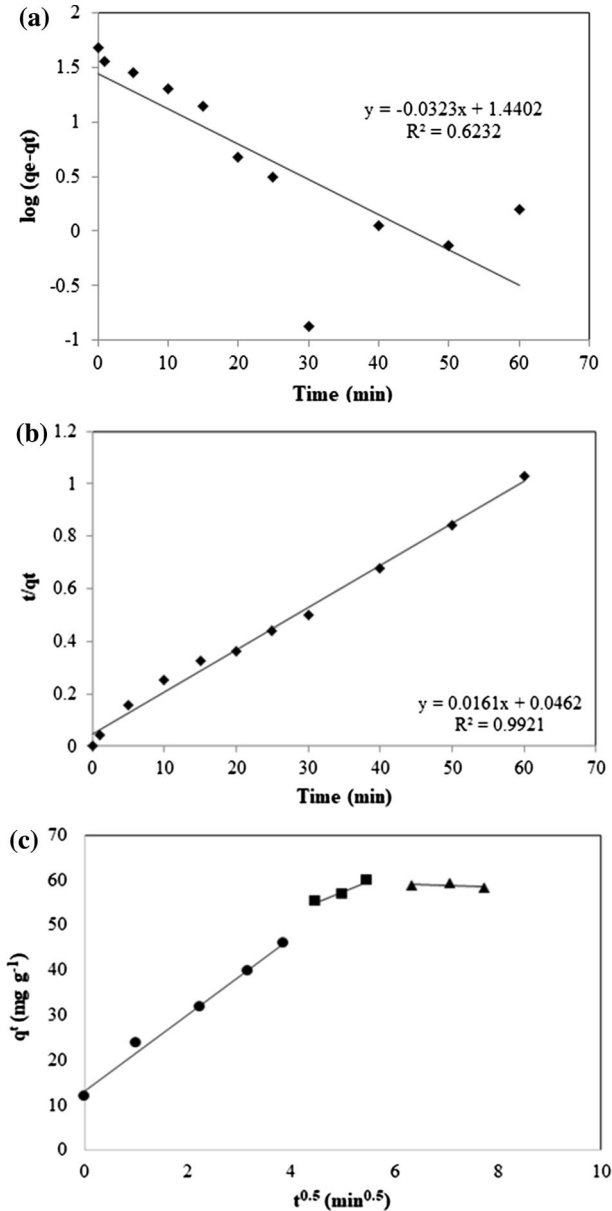


Fig. 7 **a** Pseudo-first order model fitted to the MB adsorption data; **b** pseudo-second order model fitted to the MB adsorption data and **c** intra-particle diffusion plot

The data obtained through the experiments were further evaluated using a pseudo-second-order kinetic model (Eq. (6)) [17]:

$$\frac{t}{q_t} = \frac{1}{k_2 q_e^2} + \frac{t}{q_e} \quad (6)$$

k_2 ($\text{g mg}^{-1} \text{min}^{-1}$) being the second-order rate constant. A plot of t/q_t versus time gives a straight-line, with the respective slope and intercept of $1/q_e$, and $1 = k_2 q_e^2$. The equation gives the rate constant (k_2) and the equilibrium amount of the adsorbed species ($q_{e,\text{cal}}$) (Fig. 7).

Based on the regression coefficients in Table 3, the adsorption of MB on the YTNPs was found to follow a pseudo-second-order model.

To evaluate the mechanism for the diffusion of MB molecules, the intra-particle diffusion model suggested by Weber and Morris was used, according to which the amount of the adsorbed species is given by Eq. (7) [55]:

$$q_t = K_{\text{id}} t^{0.5} + C \quad (7)$$

In this equation, k_i ($\text{mg g}^{-1} \text{min}^{0.5}$) illustrates the intra-particle diffusion rate constant, and can be determined from the slope of the linear plot of q_t versus $t^{0.5}$. In the case of solid–liquid adsorption processes, the solute transfer is characterized either as being an external mass transfer (boundary layer diffusion) or an intra-particle diffusion phenomenon, or a hybrid of the two. The transport of the MB occurs through the steps of: (1) film diffusion, i.e., moving from bulk solution through the liquid film to the surface of the YTNPs, (2) intra-particle diffusion, i.e., moving within the pores of the sorbent, and (3) pore diffusion, i.e., an ion-exchange reaction or the interaction of the MB with an active surface site.

Based on the experimental data (Fig. 7), which exhibit multi-linear plots, three steps can affect the sorption process. In the first of these, the immediate adsorption leads to the sharper part of the graph. The intra-particle diffusion, at this stage, is not the only rate-determining step and other steps like the boundary layer adsorption might affect the adsorption rate [56, 57]. Upon increasing the dye concentration, the slope of the plot increases, showing that, at high concentrations, a multitude of dye molecules will interact with the active sites of the YTNPs and a high adsorption intensity is observed.

Once all the external active sites are occupied, the dye molecules tend to enter the sorbent pores [58]. Furthermore, the adsorption slowly diminishes in the second and third linear portions of the curves, and, based on what is said above, the intra-particle diffusion becomes a dominant phenomenon. Eventually, the curves corresponding to the different concentrations refer to reaching the final equilibrium stage, wherein the intra-particles diffusion slows down because of extremely low MB concentration in solution.

Furthermore, the diffusion rate constants at each concentration change are in the order of $k_{i,1}$, 8.50, $> k_{i,2}$, 4.56, $> k_{i,3}$, – 0.31, the first reflecting the fastest. The fact that the $k_{i,1}$ for the adsorption of MB on the YTNPs is much higher than the others can reflect the existence of fresh active sites on the surface of the YTNPs [59]. On the other hand, the increases in the intercept values (61.05, 34.59, and 13.10) are

time-dependent as a result of the increase in the boundary layer diffusion [60], since MB molecules enter the sorbent pores. As a result, the MB adsorption mechanism is rather convoluted since both the surface adsorption and intra particle diffusion phenomena contribute to the overall process.

Isothermal studies on the adsorption

The well-known Langmuir and Freundlich isotherm models were used to simulate the experimental results. Figure 8 illustrates the isotherms obtained for the sorption of MB on the YTNPs at various temperatures, as well as the effect of the initial MB concentrations on the adsorption phenomenon at 25 °C. It can be clearly seen that the adsorption capacity of YTNPs is sharply enhanced and reaches a plateau, which is because, when the initial MB concentration is high enough (> 200 ppm), YTNPs can be saturated with MB. The results revealed that, under equilibrium conditions, the capacity for adsorbing MB increased from 16.1 to 58.9 mg g⁻¹ upon increasing the initial MB concentration in the range of 50–300 ppm.

Increasing the initial MB concentration creates a driving force to overcome resistance against the transfer of MB between the aqueous and solid phases, enhancing the mass transfer of MB molecules from the bulk solution to the surface of the YTNPs [61]. In the case of adsorption systems, the data fitted very well to the linear Langmuir isotherm:

$$\frac{C_e}{q_e} = \frac{1}{K_L q_m} + \frac{C_e}{q_m} \quad (8)$$

q_m and K_L are the maximum monolayer capacity of the sorbent (mg g⁻¹), and K is the Langmuir adsorption constant (L mg⁻¹) which is a function of the adsorption free energy. The logarithmic form of the well-known Freundlich isotherm, on the other hand, is expressed by [62]:

$$\ln(q_e) = \ln(K_F) + \frac{1}{n} \ln(C_e) \quad (9)$$

in which K_F (L mg⁻¹) and n represent the adsorption capacity of the sorbent and an index of the favorability of the adsorption process. These are Freundlich constants with n values between 2 and 10; 1 and 2 and less than 1 indicate good, difficult and poor adsorption characteristics. In the case of the present study, n was in the good ($2 < n < 10$) region (Table 3). Figure 8 shows the adsorption isotherms of the dye on YTNPs.

The correlation coefficients of the isotherm constants for the linear Langmuir and Freundlich equations have been presented in Table 4. The regression coefficients obtained from the linearized isotherms indicated that the data fitted the Langmuir isotherm to a better degree, suggesting that, once MB molecules occupy the sites throughout the surface of the YTNPs, the adsorption is completed, and hence a monolayer of MBs can be formed.

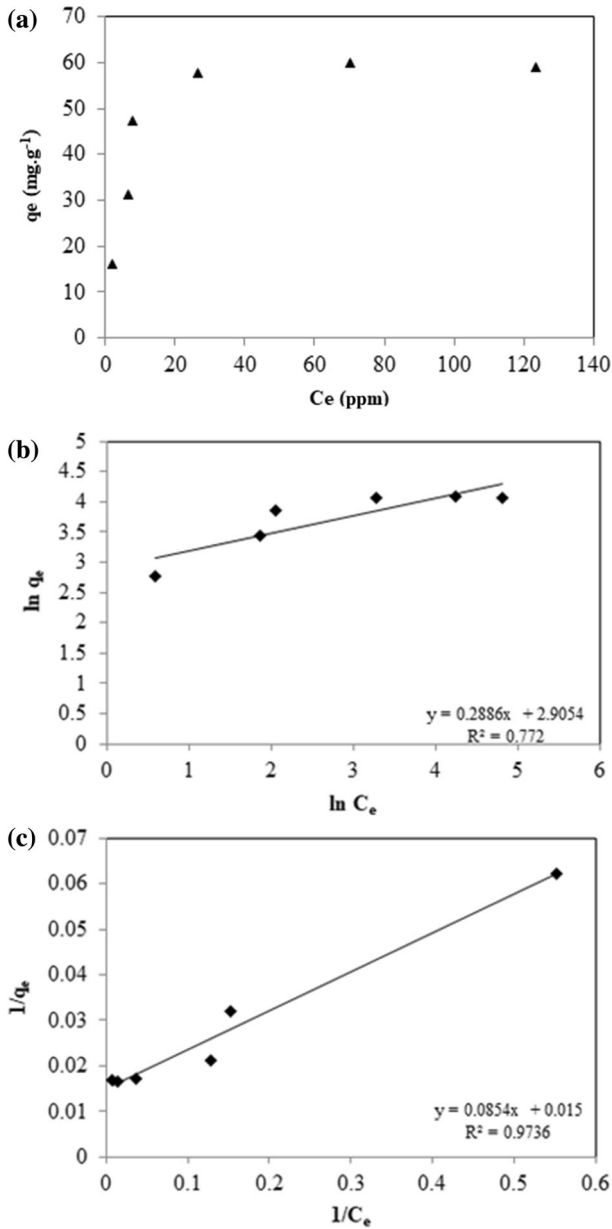


Fig. 8 **a** Isotherm curve (q_e vs. C_e), **b** Freundlich model, and **c** Langmuir model for adsorption of MB

The highest adsorption capacity of the YTNPs, based on the Langmuir adsorption isotherms, was 60.7 mg g^{-1} . Also, it can be concluded that increasing the temperature does not significantly affect the adsorption phenomenon.

Table 4 Langmuir and Freundlich parameters for the adsorption of MB on YTNP s at different temperatures

<i>T</i> (K)	Langmuir constants				Freundlich constants		
	q_m	K_L	R_L	R^2	n	K_f	R^2
297	60.7	0.17	0.03	0.98	3.4	18.3	0.77

Furthermore, the suitability of the sorbent for MB was evaluated based the separation factor constant (R_L) calculated from:

$$R_L = \frac{1}{1 + K_L C_0} \quad (10)$$

where K_L and C_0 represent the Langmuir isotherm constant in $L \text{ mg}^{-1}$ and initial MB concentration in ppm, respectively. Based on the literature, the studied adsorption phenomenon is unfavorable for $R_L > 1$, is linear if $R_L = 1$, is favorable if $0 < R_L < 1$ and irreversible for $R_L = 0$ [58]. The R_L value, in this case, was 0.03 (see Table 3), reflecting the fact that adsorption is favorable.

Desorption and reusability studies

In order to investigate the reusability of the proposed YTNPs adsorbent, five repeats of the adsorption–desorption cycle were examined. The desorption process was investigated with NaCl, NaOH and HCl solutions and the results showed that NaCl (1M) was an appropriate and operational solution for this purpose. Also, the reusability investigation confirmed that the removal efficiency of YTNPs stayed above 85 and 70% in the 1st–3rd and 3rd–5th cycles, respectively. Therefore, the proposed YTNPs are an efficient adsorbent for practical water and wastewater treatments.

Treatment of real samples

The results obtained for experiments involving the removal of MB from real samples containing various amounts of the dye, together with the mean and standard deviation of the measured MB concentrations, are reported in Table 5. The results clearly show that the adsorbents can efficiently remove MB from the slurry samples.

Table 5 MB removal from real samples by the YTNPs

Real sample	MB added (ppm)	MB removal (%)
Textile wastewater	0 ^a	–
	100	93.5 ± 10.1
	200	87.0 ± 9.8
	300	57.9 ± 12.2

^aAs-received samples

Table 6 The adsorption capacities of adsorbents with similar structures towards MB

Adsorbents	Q_m (mg g ⁻¹)	Adsorption conditions (°C)	Time (min)	Isotherm	Kinetic	Refs.
Novel magnetic Fe ₃ O ₄ @C	44.4	25	150	–	–	[64]
B-Fe ₃ O ₄ @C	42.1	30	350	Langmuir	Pseudo-second-order	[65]
Fe ₃ O ₄ @SiO ₂	33.1	25	5	Langmuir	Pseudo-second-order	[66]
Fe ₃ O ₄ @SiO ₂ @RF	45.1	30	300	Langmuir	Pseudo-second-order	[67]
Hollow CuWO ₄ spheres	59.8	25	10	Langmuir	Pseudo-second-order	[63]
YTNP _s	59.9	25	30	Langmuir	Pseudo-second-order	This work

Comparison with other works

The capability of the proposed YTNP_s for MB adsorption were compared to some of the recently reported MB adsorbents and are summarized in Table 6. As can be seen, the two tungstate adsorbents, CuWO₄ and YTNP_s, show higher adsorption capacity in comparison with the others. On the other hand, the proposed YTNP_s have an easier synthetic process in comparison with CuWO₄ [63], and especially with novel magnetic Fe₃O₄@C [64], B-Fe₃O₄@C [65], Fe₃O₄@SiO₂ [66], and Fe₃O₄@SiO₂@RF [67]. Also, the contact time of the proposed MB removal procedure is acceptable in comparison with novel magnetic Fe₃O₄@C, B-Fe₃O₄@C, Fe₃O₄@SiO₂@RF.

Conclusions

Ytterbium tungstate nanoparticles (YTNP_s) were used as a sorbent for methylene blue (MB). The initial experiments indicated that three factors influence the MB removal efficiency, and hence, to maximize this factor, a statistical experimental design method was used to optimize the adsorption of MB as a model cationic dye. Based on the results, the pH of the sample solution and the amount (dose) of the sorbent have a negative effect on the removal efficiency, while contact time has a positive effect on the outcome at low pH and high sorbent doses. However, contact time was found to have a negative effect at high pH values and low sorbent doses. The final results indicated that YTNP_s are promising materials for use as a novel sorbent for the removal of similar dye pollutants from water samples.

References

1. D. Pokhrel, T. Viraraghavan, *Sci. Total Environ.* **333**, 1 (2004)
2. S. Fan, H. Li, Y. Wang, Z. Wang, J. Tang, J. Tang, X. Li, *Res. Chem. Intermed.* **44**, 1 (2018)
3. C. O'Neill, F.R. Hawkes, D.L. Hawkes, N.D. Lourenço, H.M. Pinheiro, W. Delée, *J. Chem. Technol. Biotechnol.* **74**, 11 (1999)

4. M. Vijaykumar, P.A. Vaishampayan, Y.S. Shouche, T. Karegoudar, *Enzyme Microb. Technol.* **40**, 2 (2007)
5. A. Zahrim, C. Tizaoui, N. Hilal, *Desalination* **266**, 1 (2011)
6. Q. Wang, D. Gao, C. Gao, Q. Wei, Y. Cai, J. Xu, X. Liu, Y. Xu, *Int. J. Photoenergy* (2012)
7. C.-H. Liu, J.-S. Wu, H.-C. Chiu, S.-Y. Suen, K.H. Chu, *Water Res.* **41**, 7 (2007)
8. A. Bouazizi, M. Breida, B. Achiou, M. Ouammou, J.I. Calvo, A. Aaddane, S.A. Younsi, *Appl. Clay Sci.* **149**, 127 (2017)
9. B.K. Körbahti, K. Artut, C. Geçgel, A. Özer, *Chem. Eng. J.* **173**, 3 (2011)
10. C. Liu, Y. You, R. Zhao, D. Sun, P. Zhang, J. Jiang, A. Zhu, W. Liu, *Ecotoxicol. Environ. Saf.* **145**, 8 (2017)
11. W. Konicki, A. Helminiak, W. Arabczyk, E. Mijowska, J. Colloid Interface Sci. **497**, 155 (2017)
12. T. Robinson, G. McMullan, R. Marchant, P. Nigam, *Bioresour. Technol.* **77**, 3 (2001)
13. G. Crini, *Bioresour. Technol.* **97**, 9 (2006)
14. K. Hemashree, J.I. Bhat, *Res. Chem. Intermed.* **43**, 8 (2017)
15. P.S. Thue, G.S. dos Reis, E.C. Lima, J.M. Sieliechi, G. Dotto, A.G. Wamba, S.L. Dias, F.A. Pavan, *Res. Chem. Intermed.* **43**, 2 (2017)
16. A. Mittal, J. Mittal, A. Malviya, V. Gupta, *J. Colloid Interface Sci.* **340**, 1 (2009)
17. E. Repo, J.K. Warchoł, A. Bhatnagar, A. Mudhoo, M. Sillanpää, *Water Res.* **47**, 14 (2013)
18. G. Crini, P.-M. Badot, *Prog. Polym. Sci.* **33**, 4 (2008)
19. Y.C. Sharma, *J. Chem. Eng. Data* **55**, 1 (2009)
20. S. Wang, Z. Zhu, A. Coomes, F. Haghseresht, G. Lu, *J. Colloid Interface Sci.* **284**, 2 (2005)
21. I. Khurana, A. Saxena, J.M. Khurana, P.K. Rai, *Water Air Soil Pollut.* **228**, 5 (2017)
22. J.-Z. Sun, Z.-H. Liao, R.-W. Si, G.P. Kingori, F.-X. Chang, L. Gao, Y. Shen, X. Xiao, X.-Y. Wu, Y.-C. Yong, *Wat. Sci. Tech.* **70**, 10 (2014)
23. M. Aghazadeh, I. Karimzadeh, M.R. Ganjali, *Phys. Status Solidi A* **214**, 11 (2017)
24. A.S. Dezfuli, M.R. Ganjali, H. Jafari, F. Faridbod, *J. Mater. Sci.-Mater. Electron.* **28**, 8 (2017)
25. A.S. Dezfuli, M.R. Ganjali, H.R. Naderi, *Appl. Surf. Sci.* **402**, 245 (2017)
26. S.M. Pourmortazavi, M. Rahimi-Nasrabadi, M. Aghazadeh, M.R. Ganjali, M.S. Karimi, P. Norouzi, *J. Mol. Struct.* **1150**, 411 (2017)
27. S.M. Pourmortazavi, M. Rahimi-Nasrabadi, M. Aghazadeh, M.R. Ganjalie, M.S. Karimie, P. Norouzie, *Desalin. Water Treat.* **74**, 316 (2017)
28. H.R. Naderi, A. Sobhani-Nasab, M. Rahimi-Nasrabadi, M.R. Ganjali, *Appl. Surf. Sci.* **423**, 1025 (2017)
29. A. Sobhani-Nasab, H. Naderi, M. Rahimi-Nasrabadi, M.R. Ganjali, *J. Mater. Sci.-Mater. Electron.* **28**, 12 (2017)
30. M. Rahimi-Nasrabadi, V. Pourmohamadian, M.S. Karimi, H.R. Naderi, M.A. Karimi, K. Didehban, M.R. Ganjali, *J. Mater. Sci.-Mater. Electron.* **28**, 12391 (2017)
31. M. Rahimi-Nasrabadi, S.M. Pourmortazavi, M.R. Ganjali, A.R. Banan, F. Ahmadi, *J. Mol. Struct.* **1074**, 85 (2014)
32. M. Rahimi-Nasrabadi, S.M. Pourmortazavi, M.R. Ganjali, P. Norouzi, F. Faridbod, M.S. Karimi, *J. Mater. Sci.-Mater. Electron.* **28**, 3325 (2017)
33. M. Shoghi-Kalkhoran, F. Faridbod, P. Norouzi, M.R. Ganjali, *J. Mater. Sci.-Mater. Electron.* **29**, 1 (2018)
34. Z. Tang, L. Zhou, F. Wang, L. Zhou, *Spectrochim. Acta A* **72**, 2 (2009)
35. S.M. Pourmortazavi, M. Rahimi-Nasrabadi, M.R. Ganjali, M.S. Karimi, P. Norouzi, F. Faridbod, *Open Chem.* **15**, 1 (2017)
36. C. Venkateswarlu, G.H. Kumar, M. Seshadri, Y. Ratnakaram, K.K. Rao, J. Rao, *J. Alloys Compd.* **502**, 1 (2010)
37. J. Chen, X. Gong, Y. Lin, Y. Chen, Z. Luo, Y. Huang, *J. Alloys Compd.* **492**, 1 (2010)
38. X. Yang, X. Yu, H. Yang, Y. Guo, Y. Zhou, *J. Alloys Compd.* **479**, 1 (2009)
39. W. Guo, Y. Lin, X. Gong, Y. Chen, Z. Luo, Y. Huang, *Appl. Phys. B* **94**, 1 (2009)
40. L. Tian, S.-I. Mho, *Solid State Commun.* **125**, 11 (2003)
41. M. Rahimi-Nasrabadi, S.M. Pourmortazavi, M.S. Karimi, M. Aghazadeh, M.R. Ganjali, P. Norouzi, *J. Mater. Sci.-Mater. Electron.* **28**, 9 (2017)
42. S.M. Pourmortazavi, M. Rahimi-Nasrabadi, M. Aghazadeh, M.R. Ganjali, M.S. Karimi, P. Norouzi, *Mater. Res. Express* **4**, 3 (2017)
43. D.P. Dutta, A. Rathore, A. Ballal, A. Tyagi, *RSC Adv.* **5**, 115 (2015)
44. D.P. Dutta, A. Mathur, J. Ramkumar, A.K. Tyagi, *RSC Adv.* **4**, 70 (2014)

45. A. Singh, D.P. Dutta, J. Ramkumar, K. Bhattacharya, A.K. Tyagi, M. Fulekar, RSC Adv. **3**, 44 (2013)
46. D.P. Dutta, A. Singh, A. Ballal, A.K. Tyagi, Eur. J. Inorg. Chem. **2014**, 33 (2014)
47. M. Rahimi-Nasrabadi, S.M. Pourmortazavi, M. Aghazadeh, M.R. Ganjali, M.S. Karimi, P. Norouzi, J. Mater. Sci.-Mater. Electron. **28**, 11 (2017)
48. D.C. Montgomery, *Design and Analysis of Experiments* (Wiley, Hoboken, 2017)
49. S.N. Deming, S.L. Morgan, *Experimental Design: A Chemometric Approach* (Elsevier, New York, 1993)
50. A.R. Bagheri, M. Ghaedi, A. Asfaram, R. Jannesar, A. Goudarzi, Ultrason. Sonochem. **35**, 112 (2017)
51. E.A. Dil, M. Ghaedi, A. Ghaedi, A. Asfaram, A. Goudarzi, S. Hajati, M. Soylyak, S. Agarwal, V.K. Gupta, J. Ind. Eng. Chem. **34**, 186 (2016)
52. A. Asfaram, M. Ghaedi, M.A. Azqhandi, A. Goudarzi, M. Dastkhooon, RSC Adv. **6**, 46 (2016)
53. R.L. Mason, R.F. Gunst, J.L. Hess, *Statistical Design and Analysis of Experiments: With Applications to Engineering and Science* (Wiley, Hoboken, 2003)
54. M.N. Sepehr, V. Sivasankar, M. Zarrabi, M.S. Kumar, Chem. Eng. J. **228**, 192 (2013)
55. W. Weber, J. Morris, Adv. Water Pollut. Res. **2**, 231 (1962)
56. S. Hosseini, M.A. Khan, M.R. Malekbala, W. Cheah, T.S. Choong, Chem. Eng. J. **171**, 3 (2011)
57. H. Qiu, L. Lv, B.-C. Pan, Q.-J. Zhang, W.-M. Zhang, Q.-X. Zhang, J. Zhejiang Univ. Sci. A **10**, 5 (2009)
58. Y. Ren, H.A. Abbood, F. He, H. Peng, K. Huang, Chem. Eng. J. **226**, 300 (2013)
59. A.R. Nestic, S.J. Velickovic, D.G. Antonovic, J. Hazard. Mater. **209**, 209 (2012)
60. M. Doğan, Y. Özdemir, M. Alkan, Dyes Pigment. **75**, 3 (2007)
61. F.-C. Wu, R.-L. Tseng, R.-S. Juang, Water Res. **35**, 3 (2001)
62. Y. Li, K. Sui, R. Liu, X. Zhao, Y. Zhang, H. Liang, Y. Xia, Energy Procedia **16**, 863 (2012)
63. J.-F. Li, Y. Chen, Z. Wang, Z.-Q. Liu, J. Colloid Interface Sci. **526**, 459 (2018)
64. Z. Zhang, J. Kong, J. Hazard. Mater. **193**, 325 (2011)
65. Y. Shao, L. Zhou, C. Bao, J. Ma, M. Liu, F. Wang, Chem. Eng. J. **283**, 1127 (2016)
66. X. Tan, L. Lu, L. Wang, J. Zhang, Eur. J. Inorg. Chem. **2015**, 18 (2015)
67. Y. Shao, L. Zhou, C. Bao, J. Ma, Carbon **89**, 378 (2015)